Performance of handheld MIMO terminals in noise- and interference-limited urban macrocellular scenarios

Plicanic, Vanja; Asplund, Henrik; Lau, Buon Kiong

Published in:
IEEE Transactions on Antennas and Propagation

DOI:
10.1109/TAP.2012.2201072

2012

Document Version:
Peer reviewed version (aka post-print)

Performance of Handheld MIMO Terminals in Noise- and Interference-Limited Urban Macrocellular Scenarios

Vanja Plicanic, *Member, IEEE*, Henrik Asplund, and Buon Kiong Lau, *Senior Member, IEEE*

***Abstract*—Multiple-antenna handheld terminals are an integral part of the latest mobile communication systems, due to the adoption of multiple-input multiple-output (MIMO) technology. In this contribution, MIMO performances of three multiple-antenna configurations for smart phones are investigated in an urban macrocellular environment, based on an extensive MIMO measurement campaign at 2.65 GHz. The smart phones were held in a two-hand user grip position and both downlink noise- and interference-limited scenarios were evaluated. Our results show that, overall along the test route, the capacity performances are dictated by the power of the communication links. Nevertheless, locally, the multipath richness of the communication channel can have a significant impact on the capacity performances. In addition to the terminal antenna configurations, spatial and cross polarization references were also utilized to further illustrate the importance of multipath richness in both the desired and the interference channels. Moreover, the differences in the local capacity performances along the route for the three antenna configurations give a first indication of the potential benefit in implementing reconfigurable multiple antennas. If switching for maximum capacity is applied between the terminal antenna configurations in the two-hand grip position, average capacity improvements of up to 17% and 30% for local 20 m route sections are observed in the noise- and the interference-limited scenarios, respectively.**

***Index Terms*—MIMO, channel capacity, interference channels, antennas.**

I. Introduction

THE huge potential of multiple-input multiple-output (MIMO) technology to give impressive performance gains in wireless communications is now an undisputed fact [1]. This has led to it being an important feature in both existing and upcoming wireless communications systems. One such example is Long Term Evolution (LTE), which is currently being deployed worldwide. In LTE, it is mandatory for both base stations (BSs) and user terminals to be equipped with two or more (co-band) antennas for MIMO operations.

As a result of commercial rollouts of MIMO technology, implementation of multiple antennas for small user devices that are both practical and optimal is capturing growing interest in the research community [2]. Unlike conventional single-input single-output (SISO) systems, in which the antenna design for user terminal is mainly about good efficiency and omni-directional coverage, multiple antenna terminals in MIMO systems are required to facilitate spatially independent signals that enhances link reliability and/or support parallel sub-channels (*i.e.*, spatial multiplexing). Hence, the performance of a multiple antenna terminal critically depends on its interaction with the base station's multiple antennas, the propagation channel and the user. In other words, the achieved overall MIMO channel is of paramount importance.

Therefore, MIMO channel measurements have been an important approach of evaluating the overall communication channel, and in the context of this work, the terminal antenna configurations. However, the majority of the existing contributions which involve extensive outdoor and indoor measurement campaigns have considered only close-to-ideal configurations for optimizing MIMO performance [3]-[9]. Few studies involve compact terminal antenna configurations [10]-[13], and even fewer are taking into consideration the effects of user on the configurations [12], [14]. For the cases where a comparison between antenna configurations is provided, it is generally performed between mobile devices of different forms and sizes, such as laptops, mobile phones and data cards. Another common feature of these research contributions is that they are limited to noise-limited scenarios. Thus, to our knowledge, there has not been any attempt to explore measured capacity performances of realistic MIMO terminal devices, with or without the presence of a user, and in the presence of co-channel interference.

Furthermore, existing empirical studies focus on average performance over measurement routes, with the recurring

Manuscript received February 20, 2011. This work was supported by Sony Ericsson Mobile Communications AB and VINNOVA (Grant no. 2009-02969).

V. Plicanic is with Sony Ericsson Mobile Communications AB (now Sony Mobile Communications), SE-221 88 Lund, Sweden, and Department of Electrical and Information Technology, Lund University, SE-221 00 Lund, Sweden (e-mail: vanja.plicanicsamuelsson@sonymobile.com).

H. Asplund is with Ericsson AB, SE-164 83 Kista, Sweden. (e-mail: henrik.asplund@ericsson.com).

B. K. Lau is with the Department of Electrical and Information Technology, Lund University, SE-221 00 Lund, Sweden (e-mail: bklau@ieee.org).

conclusion that different terminal antenna configurations have similar capacity performance, as long as the antennas efficiencies are not very different [11], [12] . The results in [3] suggest that the performance is insensitive to the array configurations, even though each of the three monopole configurations used in the study explores one or a combination of different diversity mechanisms (*i.e.*, spatial, angle and polarization diversities). Nevertheless, the capacity performance of each transmit (TX)-receive (RX) configuration in the same paper exhibits *locally* different behavior along the chosen driving route due to different antenna-channel interactions in the non-stationary propagation environment. The local variation of the capacity has been previously highlighted in [15], [16] and further analyzed in [17] for close-to-ideal antenna configurations.

In this contribution, we investigate the MIMO performances of three simple dual-antenna topologies that are based on the available space for antenna implementation in a realistic, typical size, smart phone prototype. To achieve this, we fabricated three prototypes that were identical except for their antenna topologies. The 2 × 2 MIMO channels between these prototypes held in a *two-hand grip position* (see Fig. 1) and each of three ±45° dual-polarized BS sectors were obtained through an extensive channel measurement campaign at 2.65 GHz in a (European city) urban macrocellular environment. Our immediate interest is in downlink transmission, where the user terminal is on the RX side. This is because our setup was partly designed to study the effect of interference in the downlink. Moreover, LTE only requires downlink MIMO operation.

The primary purpose behind the evaluation is to study the potential of antenna system design as one key performance differentiator among terminals of the same form factor when utilized by a user. This study is performed by analyzing both *overall* and *local* channel performances. For closer correspondence to reality, MIMO capacity is obtained for both *noise-limited* (NL) and *interference-limited* (IL) scenarios. Whereas the noise-limited scenario is often chosen for convenience, the interference-limited scenario is more typical for urban environments with dense BS deployments. Moreover, as reference cases, two close-to-ideal reference antenna configurations were included in the same measurement campaign. We note that some preliminary results from this work, which focus on the terminal performance in the free space case, are reported in [18].

In Section II, the extensive MIMO channel measurement campaign is described in detail. In Section III, terminal and reference multi-antenna configurations and their radiation performances are presented. This is followed by a description of the evaluation methodology of this paper in Section IV. Section V provides comprehensive results, together with comments and discussions. Section VI concludes the paper.

II. Measurement Campaign

The measurements of multi-antenna communication channel were conducted with a proprietary wideband channel sounder comprising an 8-branch transmitter and a 4-branch receiver operating with a bandwidth of 20 MHz in the 2.65 GHz frequency band. The channel sounding equipment was to a large extent tailor-built to conform to the LTE standard, with one major exception that it was designed for the purpose of high quality channel estimation rather than wireless communication. The purpose is fulfilled by transmitting pilot symbols over the full bandwidth and by utilizing on-line calibration of the transmitter and receiver radio branches to eliminate amplitude and phase errors. Pilot symbols from the TX branches were time-multiplexed over 9 LTE symbols, where the 9th symbol was left unused to allow receiver calibration. Synchronization of the transmitter and receiver was achieved through the use of rubidium frequency standards. A complete snapshot of the 20 MHz, 8 × 4 MIMO channel was recorded every 5.33 ms and stored on a disk for off-line post processing and analysis. The pilot symbols for each snapshot were sent under 100 μs, which ensures that quasi-static channel estimates are obtained.

The measurement campaign was conducted in Kista, the northern part of Stockholm, Sweden. This is an urban area with predominantly five to eight stories high office buildings. The channel sounder TX branches were connected in pairs to three ±45° dual-polarized sector-covering antennas (65° beamwidth, 18 dBi gain), which were installed on the roof of a building. The roof level was at a height of 34 m above the ground level. The TX antenna configuration enables a three-sector BS site, similar to those commonly utilized in wireless cellular systems. An additional pair of omni-directional antennas, which was placed at the same site, was connected to the last pair of the TX branches, though these will not be considered further in this paper.

The 4-branch receiver was installed in a measurement van and connected to the RX antenna configurations placed on the roof of the van (see Fig. 1). Hence, two dual-antenna

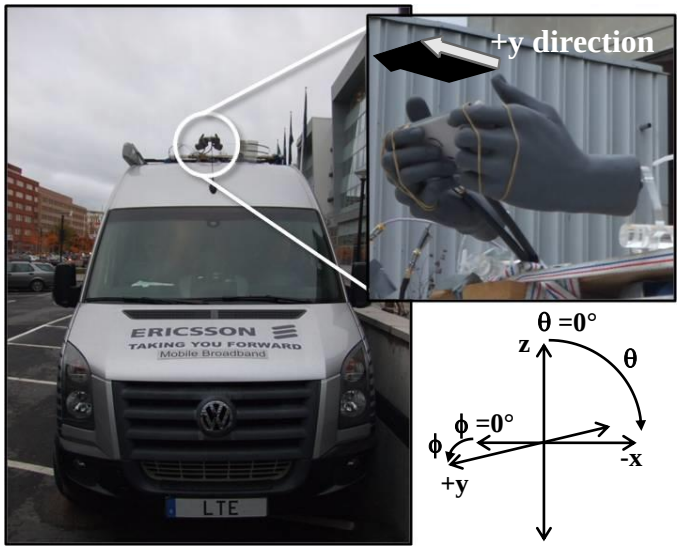

Fig. 1. A prototype in a two-hand grip position is placed on the roof of the measurement van. On the right, the detailed two-hand grip and the corresponding coordinate system used for the set-up in the field and anechoic chamber measurements are shown.

configurations were evaluated simultaneously in any given measurement. The measurements were performed with the van driving along different measurement routes within the three-sector site at speeds not exceeding 30 km/h. This was to ensure sampling of at least two measurement points per traveled wavelength, in order to obtain more data for good statistics. GPS positioning was used to simplify comparison of consecutive measurements with different antenna configurations. For simplicity and compactness of this presentation, this paper focuses on the 0 to 600 m part of a route illustrated in Fig. 2. Similar trends in results have been observed along the remaining part of this route, as well as along other measurement routes that are not shown in Fig. 2.The repeatability of the results has also been confirmed using overlapping part(s) of a given route (such as the 80 m overlap between 15 m to 95 m with 1680 m to 1760 m in Fig. 2), as well as overlaps between different routes, with the van traveling in the same direction. In addition, it is noted that the satellite picture shown in Fig. 2 is unfortunately not up to date; some new buildings are missing. Furthermore, in contrast to what the figure is showing, the parking lots were fully occupied during the measurement campaign.

III. Dual-Antenna Configurations Under Evaluation

A number of dual-antenna configurations at 2.65 GHz were evaluated in the measurement campaign. However, we only provide the technical details and results for a subset of two reference and three terminal dual-antenna configurations, since they are representative of the main findings in this paper.

The reference configurations comprise two sets of antenna configurations: (1) spatial and (2) cross polarization. The spatial reference comprises vertically-oriented half-wavelength (0.5λ) dipoles separated by 0.5λ. In the cross polarization set-up, the separation between the feeds for the vertical and the horizontal half-wavelength dipole is 0.25λ. The total radiation efficiencies for each of the antennas, as well as the correlation performance of the reference configurations, are presented in Table I. These reference configurations are designed for low correlation and balanced gains in uniform 3D angular power spectrum (APS). The spatial reference exploits spatial diversity, whereas the cross polarization reference exploits angle and polarization diversity. Since these references are well known from the literature and practical applications, their 3D radiation patterns are omitted in this paper.

Whereas the reference configurations represent close-to-ideal cases of dual-antenna design for exploiting spatial, angle and polarization diversities of the channel on the RX side, the terminal antenna configurations represent cases of practical placement of the dual co-band RX antennas in terminal-like prototypes. Each of the three terminal configurations consists of two single-band antennas of simple and well known designs placed in a given configuration on the ground plane of size 111×61 mm^2 in a prototype of size $118 \times 65 \times 11$ mm^3 (see Fig. 3). The configurations are chosen to reflect spatial and closely located cases of multiple antenna implementations. The top and bottom placed antennas in prototype A are simple

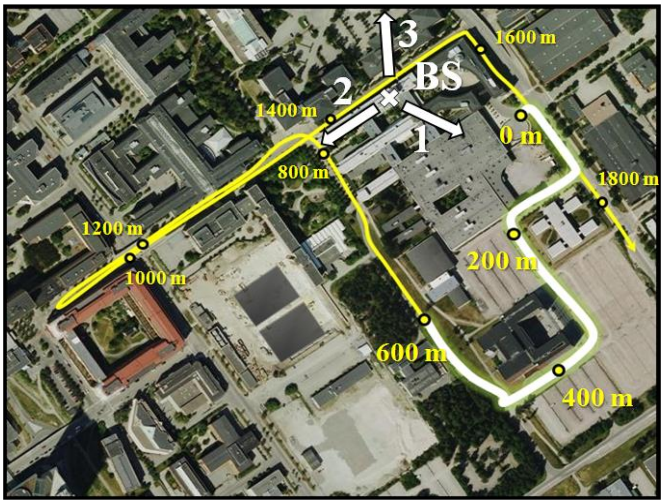

Fig. 2. Location of the BS (cross) and one driving route in the measurement campaign. Distances along the route are marked with dark circles. The thick, highlighted line marks the 600 m route under investigation. The arrows at the BS indicate the main beam directions of the TX antenna configurations for Sectors 1, 2 and 3, respectively.

TABLE I
Total Antenna Efficiencies and Envelope Correlation of the Reference Antennas and Terminal Antenna Configurations in Two-Hand Grip Position In Uniform 3D APS

Antenna configurations	Total antenna efficiency [dB]		Envelope correlation
	ANT 1	ANT 2	
Spatial reference	-1.6	-1.5	0.1
Cross pol. reference	-1.2	-1.4	0.1
A	-7.0	-6.3	0.1
B	-8.6	-9.4	0.4
C	-8.4	-7.4	0.3

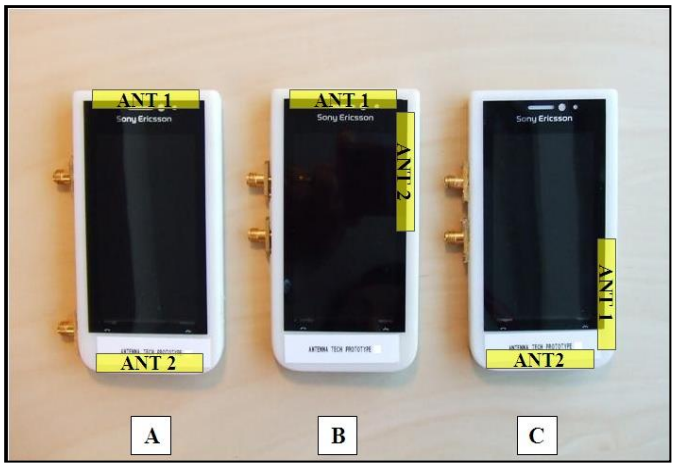

Fig. 3. Location of the antennas for each of the three multi-antenna configurations in the terminal prototypes.

folded monopole antennas. The feed separation is 95 mm (0.8λ at 2.65 GHz), and thus this configuration represents the spatial implementation case. Prototypes B and C comprise closely spaced and orthogonally placed notch antennas with feed separations of 11 mm and 6 mm (*i.e.*, less than 0.1λ at 2.65 GHz), respectively. The terminal prototypes were intended to resemble smart phones with realistic antenna implementations, and thus the antenna volume and placement were designed around a 3.5 inch display.

The terminal antenna configurations were evaluated in a user scenario of a two-hand grip position for data transfer mode, which is associated with online communication and entertainment. It is noted that the two hands case is intended to highlight the near field effects of the user. The human torso, which shadows part of the incoming waves, was not considered in this study. Figure 1 shows the handheld set-ups as installed on the roof of the van used in the measurement campaign. The coordinate system given in Fig. 1 was used in both field and antenna radiation performance measurements. Finger position markings on the back covers of all the prototypes were used to ensure repeatability in the measurements. The terminal antenna configurations were also evaluated in free space (no user) scenario and the results are presented in [18].

The total antenna efficiencies and envelope correlation in a uniform 3D APS environment are shown in Table I. Furthermore, the radiation and polarization behavior of the antennas in each of the three terminal antenna configurations in the two-hand grip position is presented in Fig. 4(a)-(f). The antenna configurations in prototypes B and C have higher correlation than the one in prototype A in the case of uniform 3D APS. The higher correlation indicates that there is more overlap in the radiation and polarization patterns of the two antennas in each of the two prototypes than those of prototype A. This is confirmed in Figs. 4(a)-(f). The cause is pattern distortion due to the presence of the user hands. The antennas in the terminal configurations are originally designed for low correlation in free space. Nonetheless, the radiation performances in Figs. 4(a)-(f) show differences in angular coverage enabled by each of the antennas in each the configurations, as well as differences in polarization states at these radiation angles. Thus, in all the three configurations, both angle and polarization diversity is exploited. Furthermore, spatial diversity is exploited in prototype A due to relatively large separation between the antenna branches.

IV. Methods of Channel Evaluation

From the original 8 × 4 MIMO channel measured along the driving route, the 2 × 2 channel matrices corresponding to the TX-RX configurations under evaluation were extracted for each of the three sectors for further post processing. Average channel gain, multipath richness and channel capacity for both noise- and interference-limited scenarios were evaluated. At each point along the route, the sector channel gains were compared and the sector with highest gain was chosen to be representative for that specific point. Hence, the channel gain, the measure of multipath richness, ellipticity statistic, and the capacity discussed further in this paper are based on switching between the sectors along the driving route. Averaging over nine wavelengths along the driving route was performed for *all* the calculated figure-of-merits in order to remove small scale fading from the data, and to enable the comparison of measurements from consecutive runs of the same route. The positional variations among these consecutive runs preclude a direct comparison on the scale of small scale fading. The averaging is limited to nine wavelengths since we found it to be the maximum distance for the channel to be wide-sense stationary (WSS) over several tested sections of the route.

A. Average Channel Gain

The average channel gain per RX branch at the *m*th measurement point is obtained from the measured 2 × 2 MIMO channel matrices $\mathbf{H}_{m,n}$ for the *m*th point and *n*th frequency subcarrier as

$$G_{MISO,m} = \left(\frac{\sum_{n=1}^{N} \left\| \mathbf{H}_{m,n} \right\|_F^2}{2N} \right), \tag{1}$$

where $\|\cdot\|_F$ denotes the Frobenius norm operator and N is number of the subcarriers in the measured bandwidth. In a 20 MHz bandwidth in this measurement campaign, 162 narrowband channel realizations were sampled at each point along the route, and thus N = 162.

B. Multipath Richness

In this paper, the relative spread (or dispersion) of the measured channel eigenvalues and thus the multipath richness in the communication channel is characterized by ellipticity statistic (ES) [19], [20], as defined by

$$\gamma^{(m,n)} = \frac{\left(\prod_{k=1}^{K} \lambda_k^{(m,n)} \right)^{\frac{1}{K}}}{\frac{1}{K} \sum_{k=1}^{K} \lambda_k^{(m,n)}}, \tag{2}$$

for the (m,n)th channel realization $\mathbf{H}_{m,n}$. The numerator is the geometric mean of the eigenvalues of $\mathbf{H}_{m,n}\mathbf{H}_{m,n}^{\dagger}$, whereas the denominator is arithmetic mean of these eigenvalues. $(\cdot)^{\dagger}$ is the conjugate transpose operator and K denotes the rank of the measured channel. $\gamma^{(i)}$ is given as a real scalar value between 0 and 1. $\gamma^{(i)} \to 1$ indicates low eigenvalue dispersion and thus high multipath richness, whereas $\gamma^{(i)} \to 0$ implies correlated sub-channels due to the lack of multipaths or polarization diversity.

C. Channel Capacity – NL Scenario

The channel capacity for $\mathbf{H}_{m,n}$ is calculated assuming no knowledge of the channel at the transmitter using [21]:

$$C_{m,n} = log_2 det \left(\mathbf{I}_2 + \left(\frac{P}{2\sigma^2} \right) \mathbf{H}_{m,n} \mathbf{H}_{m,n}^{\dagger} \right), \tag{3}$$

where $\mathbf{I}_2$ is the 2 × 2 identity matrix, σ^2 is the noise level estimated from the impulse responses of the measured sub-channels along the route and P is total transmit power. At each point along the route and for each subcarrier, the capacity was evaluated at the corresponding signal-to-noise ratio (SNR),

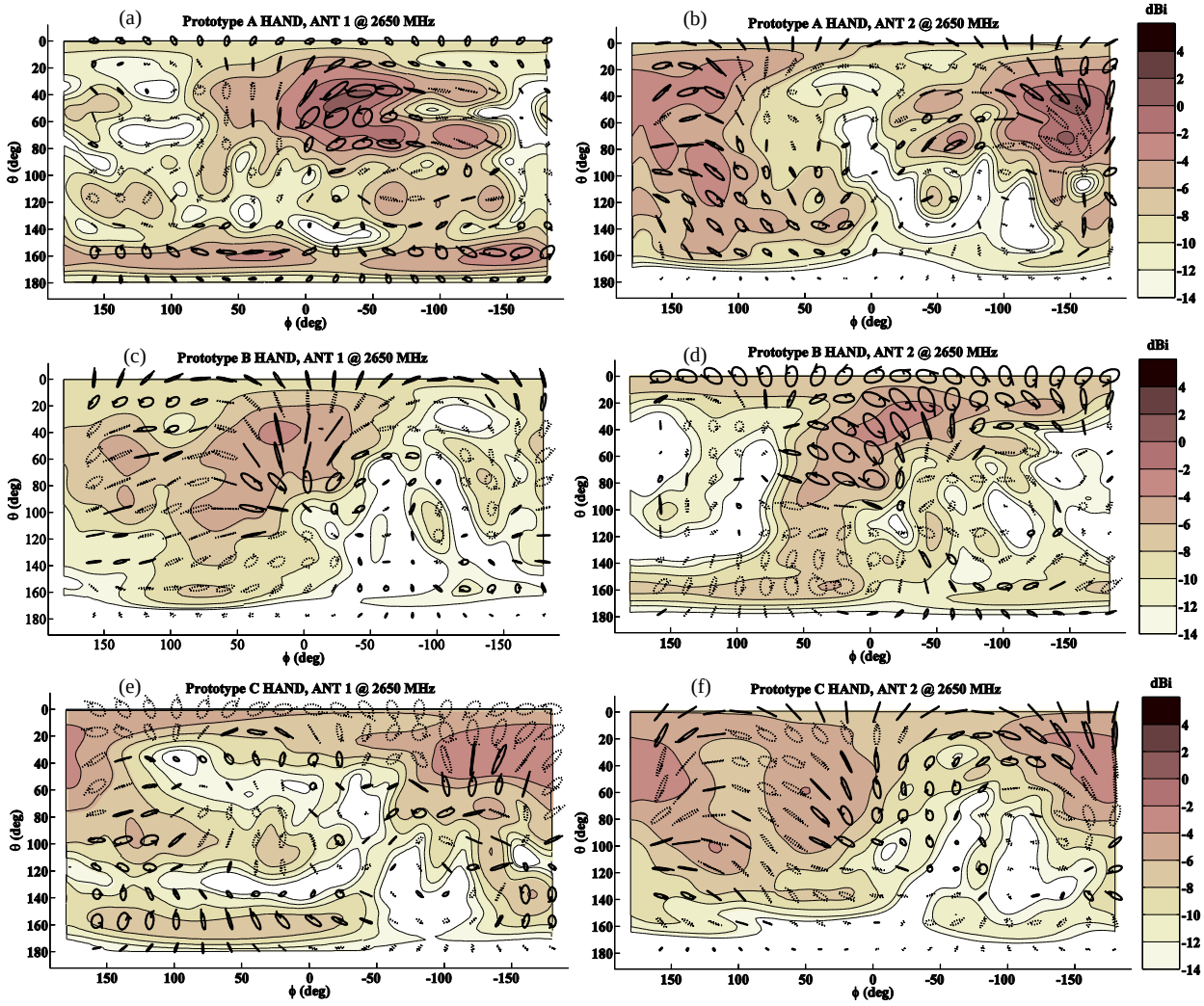

Fig. 4. 2D presentation of 3D realized gain and polarization states (dotted line circles = right hand circular polarization (RHCP), solid line circles = left hand circular polarization (LHCP)) of the two ports for each of the three prototypes A (subplots (a)-(b)), B (subplots (c)-(d)) and C (subplots (e)-(f)) at 2.65 GHz in the two-hand grip position illustrated in Fig. 1.

which for both references and all three terminal antenna configurations in handheld position was in a range of 10-45 dB. In this paper, the presented capacity results are averaged over all subcarriers [22] as well as over nine wavelengths along the route. Furthermore, where indicated, "average capacity" involves a longer section of the route (*i.e.*, 20 m) than only nine wavelengths.

D. Channel Capacity – IL scenario

The channel capacity with interference, when neither the desired channel nor the interference channel is known at the transmitter, is given in [23] as

$$C_{m,n} = log_2 det\left(\mathbf{I}_2 + \left(\frac{P}{2\sigma^2}\right)\mathbf{R}^{-1}\mathbf{H}_{m,n}\mathbf{H}_{m,n}^{\dagger}\right), \quad (4)$$

where

$$\mathbf{R} = \sum_{l=1}^{L}\left(\frac{P_l}{2\sigma^2}\right)\mathbf{H}_{m,n}^{(l)}\left(\mathbf{H}_{m,n}^{(l)}\right)^{\dagger} + \mathbf{I}_2, \quad (5)$$

and $\mathbf{H}_{m,n}^{(l)}$ is the *l*-th measured 2 × 2 interference channel matrix for the *m*th point and *n*th frequency subcarrier. P_l is the total power of the *l*-th interfering (two-antenna) sector. In this paper, two interferers are assumed (L = 2), which correspond to the channel matrices of the two (out of three) sectors with lower gains at each point along the route.

V. Analysis

The empirical data presented and discussed in this section were collected on a low traffic route during off-peak traffic hours, in an effort to avoid large propagation channel variations between test drives. Here, the repeatability of the data for the overlapping part of the route, as described in Section II and shown in Fig. 1, is quantified for the hand-held terminal measurements. The differences in received power and capacity for the overlapping part between these two runs are observed to be less than 1 dB and 0.8 bits/s/Hz, respectively. It is noted that the repeatability results for the reference antennas, omitted here for the sake of conciseness, are significantly better. Within the overlapping part, the measured SNRs are above 30 dB.

A. Reference Antenna Configurations at RX

Noise-limited (NL) scenario: The channel capacity performance of the TX-RX reference configurations in a NL scenario is shown in Fig. 5. In this case, the capacity of the cross polarization reference at the RX side is higher than that of the spatial reference for most of the route. The channel gains for these two configurations as presented in Fig. 6 are very similar, except for a few small sections along the route where the differences are up to 3 dB. Hence, the difference in the channel gains is not the predominant cause of the capacity difference. Instead, the decisive factor is the difference in the ES performances of the two reference configurations, which are presented in Fig. 7. The angular and polarization properties of the cross polarization reference at the RX side ensure high multipath richness (or high ES values) across the route, as compared to the spatial reference that is solely relying on spatial diversity. Furthermore, the cross polarization reference may also have the benefit of some spatial diversity in the multipath environment due to the 0.25λ separation between the feeds.

Two specific examples, using representative segments of the route corresponding to line-of-sight (LOS) (at 260 m) and non-line-of-sight (NLOS) propagation (at 430 m), are given here to highlight the important role of multipath richness in determining capacity performance. At 430 m, the two configurations have equal channel gains. However, the ES performances are different: ES ~0.15 and ES ~0.42 for the cases of spatial and cross polarization references, respectively. It is shown in [9], [19] that ES has a similar impact as SNR on capacity under the conditions of Rayleigh fading and high SNRs. Therefore, the spatial reference configuration in this part of the route needs an equivalent $10 \log_{10}(0.42/\ 0.15) = 4.5$ dB higher channel gain (or SNR) to compensate for the low multipath richness and thus to achieve the 15% higher capacity that is enabled with the cross polarization reference at the RX side. Higher multipath richness in NLOS is obtained through angle and polarization diversity rather than through purely spatial diversity. This is partly a result of the cross-polarized TX antenna configuration and may not be applicable in general. As a further reference, the average ES for the 2×2 Rayleigh channel is 0.59.

At 260 m, where the propagation environment is characterized by LOS propagation with angle-of-arrival (AoA) of $\phi \sim$-80° for the direct path, the capacity of the cross polarization reference configuration at the RX side is 19% higher than that of the spatial reference. As discussed by Andersen in [24], LOS propagation is often characterized by low multipath richness, which can negatively impact the capacity performance but is commonly compensated by the increase in SNR due to a dominant signal path. Note, however, that scattering in the close proximity of the terminal can cause rich multipath even in a visual LOS scenario [25]. Since the two reference configurations have similar channel gains, it can be assumed that the SNR increase due to the dominant path affects both capacity performances in a similar manner. This is also confirmed by the same Rician K-factor of 9 dB in both configurations. Thus, the capacity difference is a consequence

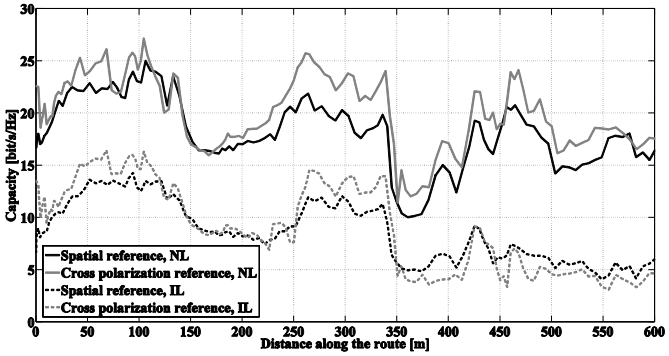

Fig. 5. Capacity performance in NL and IL scenarios of the two TX-RX configurations with reference antennas at the RX side.

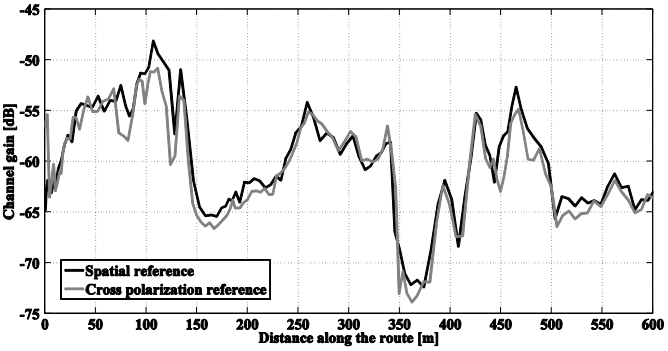

Fig. 6. Average channel gain per receive antenna and 20 MHz bandwidth for the two reference antenna configurations.

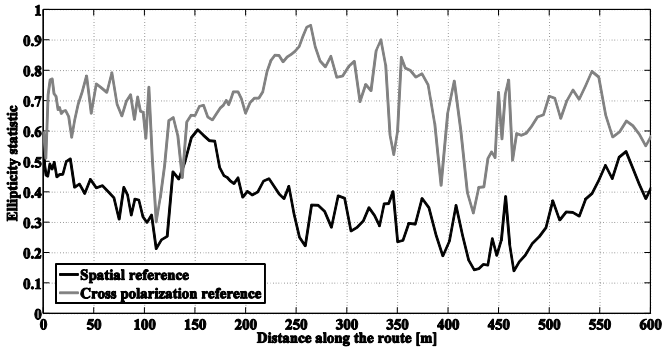

Fig. 7. Ellipticity statistic as a measure of eigenvalue dispersion for the two reference antenna configurations.

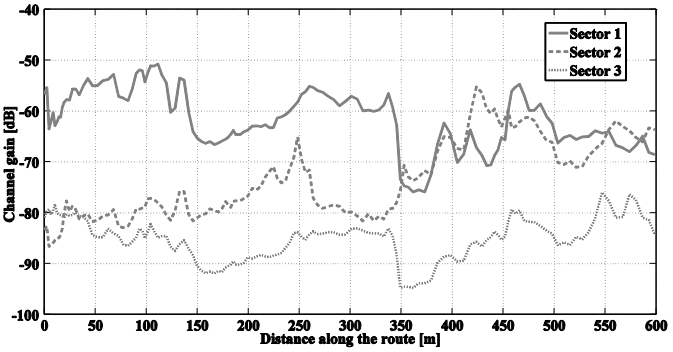

Fig. 8. Average channel gain per receive antenna and 20 MHz bandwidth for the cross polarization reference configuration at the RX side and each of the three sector antenna configurations at theTX side.

TABLE II

CHANNEL GAIN AND ELLIPTICITY STATISTIC OF DESIRED AND INTERFERENCE CHANNELS AT 400 M FOR THE TWO REFERENCE CONFIGURATIONS.

RX antenna configuration		Channel gain [dB]	ES
Spatial reference	Desired channel	-64.4	0.23
	Interference (Sector 2)	-64.9	0.29
	Interference (Sector 3)	-88.4	0.48
Cross pol. reference	Desired channel	-64.6	0.45
	Interference (Sector 2)	-65.3	0.80
	Interference (Sector 3)	-88.5	0.69

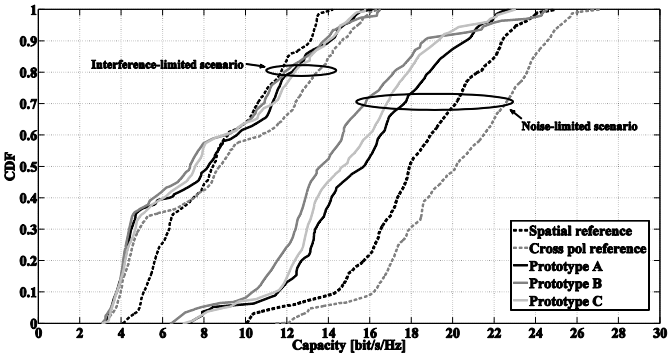

Fig. 9. Cumulative distribution function (CDF) of capacity performance in NL and IL scenarios for the TX-RX configurations with reference and handheld terminal antenna prototypes at the RX side.

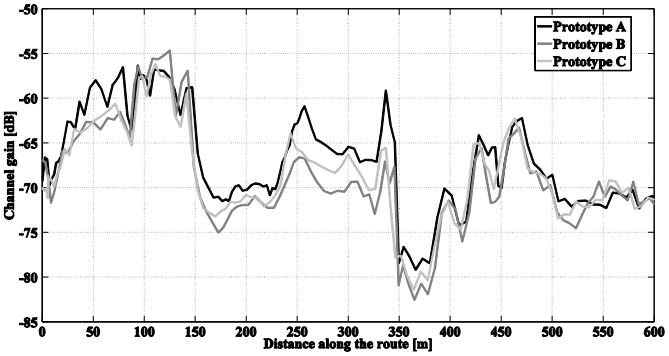

Fig. 10. Channel gain of the TX-RX configurations with handheld terminal antenna prototypes at the RX side.

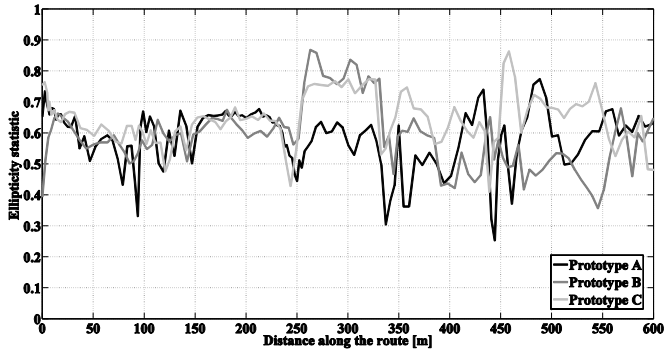

Fig. 11. Ellipticity statistic of the TX-RX configurations with handheld terminal antenna prototypes at the RX side.

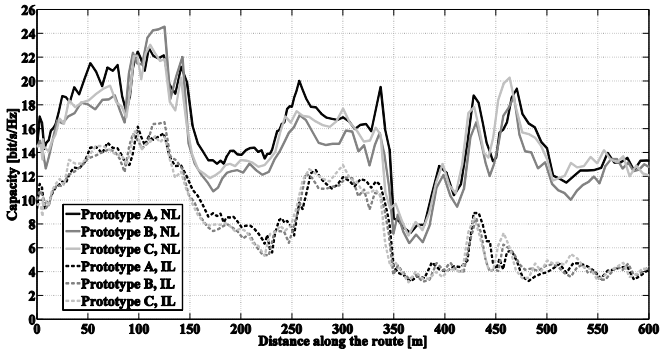

Fig. 12. Capacity performance in NL and IL scenarios with handheld terminal antenna prototypes at the RX side.

of the ES performances. Despite the obvious lack of multipath in LOS, high multipath richness (ES ~0.85) is obtained in the case of cross polarization reference at the RX side and thus higher capacity is achieved. The higher capacity is enabled by polarization diversity, and hence in this LOS case the ES is a measure of how good two orthogonal polarization sub-channels can be obtained in the communication channel.

Interference-limited (IL) scenario: The average channel gains for the cross polarization reference at the RX side and each of the three sector antenna configurations at the TX side are presented in Fig. 8. The channel gains for the three sector TX-RX configurations with the spatial reference configuration at the RX side are very similar to those presented in the Fig. 8, and thus they are omitted here. At each point along the route, the TX-RX configuration with the best channel gain is chosen as the desired channel and the remaining two configurations are used as independent 2 × 2 multi-stream interference channels. The introduction of interference with different properties along the route causes different effects on the capacity performance. At around 250 m and between 350-600 m, the channel gain of one of the two interferers is close to that of the desired channel (*i.e.*, signal-to-interference ratio (SIR) ≤ 10 dB). Hence, for both reference configurations at these parts of the route, the decrease from NL capacity performance is greater than at other parts (see Fig. 5). When compared to the capacity performances in the NL scenario, the degradation is up to 78% at SIR ≤ 10 dB and up to 45% for SIR > 10 dB.

Between 350-600 m (SIR ≤ 10 dB) the capacity of the cross polarization reference configuration at the RX side is decreased more than that of spatial reference configuration. For example, at 400 m, the decrease is 78% and 56%, respectively. Since this situation occurs over a large part of the route, the degradation can be observed in the overall average results on the route (see Fig. 9). In the case of cross polarization reference, both the desired channel and the dominant interference (from Sector 2) have different ES performances (see Table II). Moreover, at this NLOS point on the route, the interference channel has higher ES, and thus the desired channel experiences interference with high multipath richness, *i.e.*, spatially white interference. On the other hand, both the desired and dominant interference channels for the

TABLE III
AVERAGE CAPACITY FOR 20 M ROUTE SECTIONS: B FOR THE NL SCENARIO AND A FOR THE IL SCENARIO.

Route section (20 m)	RX antenna configuration	Average capacity (NL) [bit/s/Hz]	Average capacity (IL) [bit/s/Hz]
@ 260 m (LOS)	A	18.9	9.1
	B	16.8	10.7
	C	17.0	10.9
@ 460 m (NLOS)	A	16.2	5.0
	B	16.9	5.3
	C	19.4	6.5
@ 520 m (NLOS)	A	11.5	4.2
	B	10.6	3.9
	C	12.4	4.9

spatial reference have similar low ES, which implies that colored interference is introduced in a desired channel of low multipath richness. This means that the case of white interference in the multipath rich desired channel at this NLOS point degrades capacity more than the case of colored interference in the low richness desired channel. This phenomenon can be understood in that the angular spread is small in both the low richness desired channel and colored interference channel. As a result, there is a higher probability that the angles of arrival and departure of the multipath components between the desired and interference channels do not align, as compared to the multipath rich channel with white interference. Since the misalignment allows for more effective interference suppression, the capacity of the spatial reference does not decrease as much as that of the cross polarization reference. Therefore, the ES of both the desired channel and the interference channel are decisive of the resulting capacity performance. Whereas a rich multipath channel is of interest when there is no or low interference, a less dispersive desired channel can be beneficial when the interference is high and spatially colored.

B. Handheld Terminal Antenna Configurations at RX

NL scenario: Over the entire 600 m route, prototype A generally performs better than prototypes B and C in the NL scenario (see Fig. 9). At the outage probability of 50%, prototype A at the RX side enables 16% higher capacity than prototype B, which has the worst average performance. In contrast to the reference cases where the capacity performance differences are due to large differences in ES between the configurations, the handheld prototype cases show significant differences in channel gains (see Fig. 10) and smaller differences in ES performances along the 600 m route (see Fig. 11).

Fig. 12 illustrates diverse capacity performance behaviors of the terminal antenna configurations locally along the route, which result from their interactions with different propagation conditions. In the first 250 meter of the route, the ES performances are very similar for all three handheld prototypes (see Fig. 11), and hence the capacity performances are mainly decided by the channel gains. Thereafter, the differences in multipath richness are more prominent. For the purpose of understanding these local performances, three 20 m sections (with center points at 260 m, 460 m and 520 m) are chosen to be representative of our findings. Here, the local performance is represented by the average capacity for each of these 20 m sections. The length and positions of the sections are chosen such that propagation characteristics along the short distances are consistent, with regards to K-factor and visual propagation scenario. The local performances for the NL scenario are shown in Table III. To further investigate the capacity behavior of these terminals over even shorter route sections, the average capacities are also compared for 1 m route sections. The averaging over the 1 m sections corresponds to the removal of small scale fading by averaging over nine wavelengths at the three chosen center points. As previously noted, the nine wavelengths are appropriate for WSS assumption to be valid over several tested sections of the route. Since the same post-processing procedure is performed for all the presented figure-of-merits in this paper (unless otherwise mentioned), these average capacity values are readily available from Fig. 12 and thus not presented separately.

At 260 m, where the propagation environment is characterized by LOS, the best performance is obtained with prototype A at the RX side. This case gives up to 12% higher performance, as compared to prototypes B and C (see Table III). The performance over the 1 m section gives a "peak capacity improvement" of 14%. At the center point of the section where this peak improvement is achieved, prototype A has about 5 dB higher channel gain than prototypes B and C. Prototypes B and C have similar channel gains (*i.e.*, difference of less than 0.5 dB) as well as similar ES (ES (B) ~0.82, ES (C) ~0.74). The low channel gains and high ES values suggest that prototypes B and C collect less power through the dominant signal path. This is confirmed using Rician K-factor. The K-factors for B and C are below 1 dB, whereas A has a K-factor of 5.4 dB. This correlates well with the 5 dB higher channel gain and less pronounced multipath richness (ES ~0.55) in the case of prototype A at the RX side. Hence, at this local LOS section, it is power that is decisive of capacity performance. Prototype A has higher total antenna efficiencies, as well as angular and polarization patterns that are better aligned with the incoming dominant path at $\phi \sim$-80° (see Fig. 4(a)-(f)), and thus more power is collected.

At 460 m (NLOS), it is prototype C at the RX side that enables the highest capacity. The average capacity is 20% higher than that of prototype A with the lowest capacity (see Table III). Compared to prototype B, the capacity of prototype A is 15% higher. The peak capacity improvement over the 1 m section centered at 460 m is 22%. In contrast to the previous case where the power is decisive of the capacity performance, the prototypes offer similar channel gains at this location. In particular, prototype C gives 0.5 dB higher channel gain than A, which in turn provides 0.5 dB higher channel gain than B. Considering the accuracy of the measurements, the channel gain performances can be assumed to be practically the same. However, the ES values are significantly different among the prototypes: A has ES ~0.39, prototype B ES ~0.49 and C the highest multipath richness with ES ~0.83. Prototype C has 10

TABLE IV
SIR AND ELLIPTICITY STATISTIC OF DESIRED AND INTERFERENCE CHANNELS AT 1 M SECTIONS OF THE ROUTE, AND THEIR EFFECT ON CAPACITY FOR THE HANDHELD TERMINAL PROTOTYPES AT THE RX SIDE.

Route section (1 m)	RX antenna configuration	SIR [dB]	ES (desired channel)	ES (interference channel)	Capacity decrease [%]
@ 260 m (LOS)	A	14	0.55	0.42	52
	B	16.5	0.83	0.59	35
	C	18	0.74	0.66	32
@ 460 m (NLOS)	A	7.9	0.39	0.66	67
	B	7.9	0.49	0.63	66
	C	6.4	0.84	0.55	65
@ 520 m (NLOS)	A	4	0.5	0.65	65
	B	3.5	0.5	0.63	65
	C	5.5	0.68	0.63	60

$\log_{10}(0.84/0.39) = 3.3$ dB advantage in multipath richness, as compared to A and $10\log_{10}(0.84/0.49) = 2.3$ dB advantage in multipath richness over B. Thus, the capacity performances at this local route section mainly reflect the ES of the RX configurations.

At yet another NLOS section, at 520 m, prototype C has the best capacity performance, which is 17% better than that of prototype B (see Table III). The peak capacity improvement found at this location over the 1 m section is 29%. At this point, prototype C has ES ~0.68 and approximately 2.3 dB higher channel gain than prototype B with ES~0.5. Hence, prototype C has $10\log_{10}(0.68/0.5) = 1.3$ dB advantage in multipath richness, and thus 2.3 + 1.3 = 3.6 dB net advantage over prototype B. Here, it is the combination of both power and multipath richness that ensures superior capacity performance. Prototype A with ES ~0.5 has similar channel gain as prototype C, and hence its lower capacity is due to its higher ES.

IL scenario: In contrast to the NL scenario, in which prototype A gives the best performance both on average over the entire 600 m route and for nearly all outage probabilities, the three prototypes facilitate more similar performances in the IL scenario (see Fig. 9). However, at the outage probability of 50%, prototype A offers 12% higher capacity than prototype B, which has the worst performance. The channel gains of the desired and interference channels for all three prototypes follow the same trend as those presented for the reference cases in Fig. 8, and thus they are not graphically depicted here. Over the 600 m route, the strongest interference is observed at 250 m and 350-600 m with SIR $\leq$ 12 dB. In comparison to the NL scenario, the degradation in 50% outage capacity over the 600 m route is around 45%, 46% and 48% for prototypes A, B, and C, respectively (see Fig. 9). On the other hand, the 10% outage capacities of the three prototypes are degraded by 67%, 63% and 67%, respectively. The larger degradation for the lower outage probability is due to low SIRs at the parts of the route where capacity is lower in the NL scenario.

Local capacity performances for the IL scenarios (over 20 m route sections) are also presented in Table III. At the LOS section centered at 260 m, the best capacity performance is not obtained by prototype A, as in the NL scenario. On the contrary, prototype A shows the highest decrease in local average capacity, 52% compared to 37% and 36% for B and C, respectively, due to introduction of interference. To gain more insight of the effect of interference on capacity performance, the decrease in capacity as well as the desired and interference channel properties over three 1 m sections, are summarized in Table IV. At 260 m, prototype A experiences the highest interference, since it has the lowest SIR. From the NL scenario discussion, we know that prototype A has the highest efficiencies and also angular and polarization properties that are much more aligned with the direct (dominant) signal path than the other prototypes. Since this alignment likewise occurs in the interference channel, prototype A achieves the lowest ES in both the desired and interference channels. Moreover, given that the desired and interference direct paths are both aligned at AoA of ϕ ~-80°, the lack of orthogonality between the desired and interference channels contributes to poorer interference suppression. In addition, despite that prototype B has 1.5 dB lower SIR than C, similar capacity decrease is observed. The ES results in Table IV suggest that the larger difference in ES between the desired and interference channels in prototype B compensates for its lower SIR by enabling better interference suppression.

At 460 m (NLOS), the capacity performances of prototypes A and B are similarly degraded due to the same SIR and closely similar desired and interference channel ES values (see Table IV). In the case of prototype C, the SIR is 1.5 dB lower, and thus the capacity degradation as compared to the noise-limited case is expected to be higher. However, the lower SIR is compensated by the higher ES of the desired channel and the lower ES of the interference channel for C, relative to the other two prototypes. In other words, the larger difference in the multipath richness between the desired and interference channels facilitates more effective interference suppression. Therefore, it can be concluded that different mechanisms are responsible for the similar capacity decrease (*i.e.*, 65%-67%) in the three prototypes.

Similar to the 460 m case, the capacity of prototypes A and

B are degraded by the same amount at 520 m, due to similarities in the SIR and multipath richness of the desired and interference channels (see Table IV). In this case, however, the capacity of prototype C is degraded less due to higher SIR as well as higher ES in the desired channel.

The percentage differences in capacity between the three prototypes are significantly higher in the IL scenario than in the NL scenario. Over the 20 m section centered at 260 m (LOS), the average capacity of prototype C is 20% better than that of A, which has the lowest capacity. On the other hand, the capacity difference over the shorter 1 m section is up to 30%. Prototype C also performs better than the other two prototypes in the NLOS cases at 460 m and 520 m. Compared to the worst average capacity performances, it gives 30% and 26% improvement at local 20 m sections at 460 m and 520 m, respectively. The peak capacity improvements over 1 m sections are even higher, *i.e.*, 73% and 52% at 460 m and 520 m, respectively. Nevertheless, it is noted here that, despite extensive efforts to align the measurement points over multiple measurement runs of the same 600 m driving route, very high accuracy cannot be guaranteed. For example, in the vicinity of the 460 m point, prototype A appears to be not very well aligned with prototypes B and C (in trend), and thus the stated peak improvement of 73% may be overestimated. However, since B and C seem to be better aligned, the peak improvements between these two cases, found to be up to 55%, may be used instead to illustrate the significantly better performance that can be achieved locally with one of the prototypes as compared to the others.

C. Adaptation to the Local Communication Channels

The LOS and NLOS route sections, presented and discussed above, show how different radiation performances of dual-antenna configurations interact with several local propagation conditions to give different capacity performances. In Table V, the average capacity differences between the best performing prototype and one *fixed* configuration for each of three 20 m route sections are summarized for both NL and IL scenarios. The results give an indication of the potential benefit in capacity performance of dual-antenna terminals from antenna system reconfigurability. If we assume hypothetically that we can switch between the three RX terminal configurations for maximum average capacity along the given 20 m section (*e.g.*, using a single structure that realizes all three dual-antenna configurations through antenna selection), average capacity improvement of up to 17% can be obtained in the NL scenario, when prototype B is chosen as the fixed reference RX configuration. In the IL scenario, the improvement is up to 30%, relative to prototype A as the fixed RX configuration. The peak capacity improvements discussed in the previous section also suggest that higher capacity gains may be achieved, if the switching is performed faster (*i.e.*, for less than 20 m).

The results in Table V suggest that antenna system reconfigurability can be used to alleviate interference. However, in a real LTE system, interference as well as power loss due to user influence are commonly combated by means of power control. Ideally, power control on all links can transform an IL scenario into a NL scenario. However, due to frequency reuse and requirements for quality-of-service, some interference is inevitable in a multiuser system like LTE. Nevertheless, power control is expected to kick-in to ensure that severe interference, as seen in some parts of the measured route, will not occur. Since our results show that adaptivity in the antenna patterns is more helpful in the IL scenario than the NL scenario, antenna system reconfigurability in the power controlled system would most likely produce results that are in-between those seen for the two extreme cases of the NL and IL scenarios.

If *instantaneous* switching for maximum capacity is applied along the entire 600 m route (*i.e.*, based on the data with fast fading averaged out), the capacity gain at 50% outage probability, compared to prototype B, is 17% and 12% for NL and IL scenarios, respectively (see Fig. 13). This improvement compares favorably to that obtained in [26] for dual variable-length reconfigurable dipoles in a simulated (noise-limited) outdoor environment. In [26], an 8% average capacity improvement is achieved at 20 dB SNR, as compared to a fixed antenna configuration. The SNR range covered by the 600 m route in this study is 10-45 dB. In addition, similar improvement as that from switching for maximum capacity is obtained by switching for maximum power in both NL and IL scenarios (see Fig. 13). This observation is also made in [27], [28] for the NL scenario. We further note that this improvement is likewise similar to the capacity gain enabled by prototype A. Prototype A gives the highest 50% outage capacity amongst the three RX configurations, due to its superior channel gain performance, rather than its ES performance. However, neither choosing the best RX configuration at a given outage level nor the switching for maximum power or capacity can reveal the advantages that are observed *locally* when switching for maximum capacity is utilized.

The presented configurations serve as simple examples to highlight the potential of adaptation, despite the fact that they are not optimized for reconfigurability (*e.g.*, the antenna patterns across different prototypes are not fully orthogonal). Moreover, the practical aspect of implementing more than two co-band antennas in small terminal devices for switching purposes may be strongly limited by the size and form factor of the terminal. Thus other ways of adaptation to the local channels should be considered. Capacity driven adaptation has recently been studied in number of contributions [26], [28]-[32], focusing on optimal and suboptimal methods for reconfiguring close-to-ideal spatial antenna configurations and providing an upper bound of the performance improvement potential. The performance improvement by reconfiguring practical compact antenna systems to give best channel performance in realistic user and propagation environments is, however, relatively unknown. Nonetheless, the simple RX configurations in this study highlight the importance of different antenna radiation characteristics for better antenna-channel interaction and thus better capacity performance.

VI. Conclusions

In this study, the results from an extensive 2×2 MIMO measurement campaign at 2.65 GHz in an urban macrocellular environment involving three compact dual-antenna topologies are presented. The topologies include one spatial and two closely spaced configurations, which are implemented in prototypes of size and form factor typical of today's smart phones. The antenna configurations were evaluated in a two-hand user grip position in NL and IL scenarios. The purpose is to study the potential of antenna system design as one key performance differentiator among terminals in a realistic usage scenario. Spatial and cross polarization configurations are also evaluated as reference cases, in order to obtain more insights.

The reference configurations show the importance of multipath richness for harvesting the potential of MIMO, when the channel gains are equal. In particular, polarization and angle diversity offers significantly higher multipath richness, and hence higher capacity, than spatial diversity in both LOS and NLOS NL scenarios. This is because correlation is expected to be significantly higher for the 0.5λ-separated co-polar dual-dipole setup in the presence of one or a few dominant paths than for the cross polarized antenna setup where orthogonal channels are achieved.

Whereas, overall for the entire driving route, the multipath richness is the decisive factor in the capacity performance of the reference configurations, the capacity performance of the handheld terminal configurations largely follows the channel gain. Hence, in general, the spatial topology in the handheld position is the best option for enabling maximum capacity, due to its antenna radiation properties that ensure the best channel gain. However, locally along the route, the multipath richness or the channel gain, or a synergy of the two, in both the desired and interference channels, enables different topologies to offer the best performance in different, local propagation conditions. These local performances highlight the importance of different antenna radiation characteristics for better antenna-channel interaction and interference suppression. The same results also give an indication of the potential in maximizing capacity through adaptation of the antenna to the channel. For the 50% outage capacity over the entire route, the switching between the three handheld antenna terminal configurations for maximum capacity gives similar performance to that of switching for maximum power, which also corresponds to the best performing terminal topology (*i.e.*, prototype A). However, a significant advantage in average capacity performance is obtained at shorter sections of the route. In particular, improvements of up to 17% and 30%, relative to one fixed antenna configuration, is observed by switching for representative 20 m route sections in NL and IL scenarios, respectively. Moreover, faster switching (*i.e.*, switching over 1 m) is found to offer even greater improvements.

Acknowledgement

The authors would like to acknowledge helpful discussions with Prof. Jørgen B. Andersen of Aalborg University and Prof. Michael A. Jensen of Brigham Young University. The authors also thank Mr. Mikael Håkansson for his support in building the prototypes and Dr. Anders Derneryd of Ericsson AB for his support in the measurement campaign.

TABLE V

Average Capacity Gain at 20 m Route Sections when the Prototype with The Best Capacity is Compared to A Fixed Configuration (B for NL Scenario and A for IL Scenario).

	Capacity improvement [%]	
Route section (20 m)	NL scenario	IL scenario
@ 260 m (LOS)	12	20
@ 460 m (NLOS)	15	30
@ 520 m (NLOS)	17	17

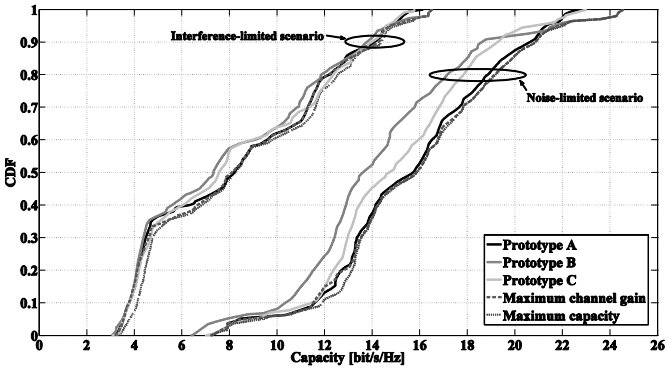

Fig. 13. CDF of capacity performance in NL and IL scenarios for each handheld terminal prototype at the RX side and when instantaneous switching for maximum channel gain and maximum capacity is applied.

References

[1] M. Jensen and J. Wallace, "A review of antennas and propagation for MIMO wireless communications," *IEEE Trans. Antennas Propagat.*, vol. 52, no. 11, pp. 2810–2824, Nov. 2004.

[2] B. K. Lau, "Multiple antenna terminals," in *MIMO: From Theory to Implementation*, C. Oestges, A. Sibille, and A. Zanella, Eds. San Diego: Academic Press, 2011, pp. 267-298.

[3] C. C. Martin, J. H. Winters, and N. R. Sollenberger, "MIMO radio channel measurements: Performance comparison of antenna configurations," in *Proc. IEEE 54th Veh. Technol. Conf.*, vol. 2, Atlantic City, NJ, Oct. 7–11, 2001, pp. 1225–1229.

[4] K. Sulonen, P. Suvikunnas, L. Vuokko, J. Kivinen, P. Vainikainen, "Comparison of MIMO antenna configurations in picocell and microcell environments," *IEEE J. Sel. Areas Commun*, vol. 21, no. 5, pp. 1-10, Jun. 2003.

[5] V. Erceg, P. Soma, D. S. Baum, and A. J. Paulraj, "Capacity obtained from multiple-input multiple-output channel measurements in fixed wireless environments at 2.5 GHz," in *Proc. IEEE Int. Conf. Commun.*, vol. 1, New York, NY, Apr. 28-May 2, 2002, pp. 396–400.

[6] K. Nishimori, Y. Makise, M. Ida, R. Kudo, and K. Tsunekawa*,"* Channel capacity measurement of 8×2 MIMO transmission by antenna configurations in an actual cellular environment," *IEEE Trans. Antennas Propagat.*, vol. 54, no. 11, pp. 3285-3291, Nov. 2006.

[7] D. Chizhik, *J.* Ling, P. W. Wolniansky, R. A. Valenzuela, *N.* Costa, and K. Huber, "Multiple-input–multiple-output measurements and modeling in Manhattan," *IEEE J. Sel. Areas Commun., vol. 21, no. 3, pp. 32*1-331, Apr. 2003.

[8] D. Uchida, H. Arai, Y. Inoue, and K. Cho, "Experimental assessment of the channel capacity in indoor MIMO systems using dual-polarization," in *Proc. IEEE 69th Veh. Technol. Conf.*, B*arcelona, Spain, Apr. 26-29,* 2009, pp. 1-5

[9] P. Suvikunnas, J. Salo, L. Vuokko, J. Kivinen, K. Sulonen, and P. Vainikainen, "Comparison of MIMO antenna configurations: methods and experimental results," *IEEE Trans. Veh. Technol.*, vol. 57, no. 2, Mar. 2008.

[10] D. W. Browne, M. Manteghi, M. P. Fitz, and Y. Rahmat-Samii, "Experiments with compact antenna arrays for MIMO radio communications," *IEEE Trans. Antennas Propagat.*, vol. 54, no. 11, pp. 3239–3250, Nov. 2006.
[11] Y. Selén, H. Asplund, "3G LTE simulations using measured MIMO channels," *in Proc. IEEE Global Telecommun. Conf.*, New Orleans, LA, Nov. 30-Dec. 4, 2008, pp.1-5.
[12] M. Hunukumbure and M. Beach, "MIMO channel measurements and analysis with prototype user devices in a 2GHz urban cell," *in Proc. IEEE 17th Int. Symp. on Personal, Indoor and Mobile Radio Commun. (PIMRC)*, Helsinki, Finland, 2006, 11-14 Sep. 2006.
[13] A. Pal, C. Williams, G. Hilton, and M. Beach, "Evaluation of diversity antenna designs using ray tracing, measured radiation patterns, and MIMO channel measurements," *EURASIP J. Wireless Commun. and Netw.*, vol. 2007, 2007.
[14] F. Harrysson, J. Medbo, A. Molisch, A. Johansson, and F. Tufvesson, "Efficient experimental evaluation of a MIMO handset with user influence," *IEEE Trans. Wireless Commun.*, vol. 9, no. 2, pp. 853-863, Feb. 2010.
[15] M. Herdin, H. Ozcelik, H. Hofstetter, and E. Bonek, "Variation of measured indoor MIMO capacity with receive direction and position at 5.2 GHz," *Electron. Lett.*, vol. 38, pp. 1283–1285, Oct. 2002.
[16] D. P. McNamara, M. A. Beach, P. N. Fletcher, and P. Karlsson, "Capacity variation of indoor multiple-input multiple-output (MIMO) channels", *Electron. Lett.*, vol. 36, pp. 2037 – 2038, Nov. 2000.
[17] E. Bonek, "MIMO propagation and channel modeling," in *MIMO: From Theory to Implementation*, C. Oestges, A. Sibille, and A. Zanella, Eds. San Diego: Academic Press, 2011, pp. 27-54.
[18] V. Plicanic, B. K. Lau, and H. Asplund , "Experimental evaluation of MIMO terminal antenna configurations in noise- and interference-limited urban scenarios," in *Proc. 5th European Conf. on Ant. and Propagat. (EUCAP)*, pp. 2756-2760, April 11-15, 2011.
[19] J. Salo, P. Suvikunnas, H. M. El-Sallabi and P. Vainikainen, "Some results on MIMO mutual information: the high SNR case," in *Proc. IEEE Global Telecommun. Conf.*, Dallas, TX, Nov.29-Dec. 3, 2004, pp. 943- 947.
[20] J. Salo, P. Suvikunnas, H. M. El-Sallabi and P. Vainikainen, "Ellipticity statistic as a measure of MIMO multipath richness," *Electron. Lett.*, vol.42, no.3, pp. 45–46, Feb. 2006.
[21] G.J. Foschini and M.J. Gans, "On limits of wireless communications in a fading environment when using multiple antennas," *Wireless Personal Communication*, vol. 6, pp. 311-335, 1998.
[22] H. Bölcskei, D. Gesbert, C. Papadias, and A. J. van der Veen, *Space Time Wireless Systems: From Array Processing to MIMO Communication*, UK: Cambridge University Press, 2006.
[23] Y. Song and S. D. Blostein, "MIMO channel capacity in co-channel interference," in *Proc. 21st Biennial Symposium on Communications*, Kingston, Canada, Jan. 2002, pp. 220–224.
[24] J. B. Andersen, "Propagation aspects of MIMO channel modelling," in *Space Time Wireless Systems: From Array Processing to MIMO Communication*, H. Bölcskei, D. Gesbert, C. Papadias, and A. J. van der Veen, , UK: Cambridge University Press, 2006, pp. 3-22.
[25] T. Svantesson and J. Wallace, "On signal strength and multipath richness in multi-input multi-output systems", in *Proc. IEEE Int. Conf. on Commun. (ICC)*, vol. 4, pp. 2683-2687, May 11-15, 2003.
[26] D. Piazza, N. J. Kirsch, R. W. Heath, A. Forenza, and K. R. Dandekar, "Design and evaluation of a reconfigurable antenna array for MIMO systems," *IEEE Trans. Antennas Propagat.*, vol. 56, no. 3, pp. 869-881, Mar. 2008.
[27] F. Harrysson, A. Derneryd, and F. Tufvesson, "Evaluation of user hand and body impact on multiple antenna handset performance," *in Proc. IEEE Int. Symp. Antennas Propagat.*, Toronto, Canada, Jul. 11-17, 2010.
[28] A. F. Molisch, M. Z. Win, Y.-S. Choi, and J. H. Winters, "Capacity of MIMO systems with antenna selection," *IEEE Trans. Wireless Commun.*, vol. 4, no. 4, pp. 1759–1772, Jul. 2005.
[29] M. A. Jensen, and M. L. Morris, "Efficient capacity-based antenna selection for MIMO systems," *IEEE Trans. Veh. Technol.*, vol. 54, no. 1, pp.110-116, Jan. 2005.
[30] D. Pinchera, J. W. Wallace, M. D. Migliore, and M. A. Jensen, "Experimental analysis of a wideband adaptive-MIMO antenna," *IEEE Trans. Antennas Propagat.*, vol. 56, no. 3, pp. 908–913, Mar. 2008.
[31] M. D. Migliore, D. Pinchera, and F. Schettino, "Improving channel capacity using adaptive MIMO antennas," *IEEE Trans. Antennas Propag.*, vol. 54, no. 11, pt. 2, pp. 3481–3489, Nov. 2006.
[32] B. A. Cetiner *et al.*, "Multifunctional reconfigurable MEMS integrated antennas for adaptive MIMO systems," *IEEE Commun. Mag.*, pp. 62–70, Dec. 2004.

Vanja Plicanic (M'07) received the M.S. and the Ph. D. degrees in electrical engineering both from Lund University, Lund, Sweden, in 2004 and 2011, respectively.

From 2004 to 2005, she was a Young Graduate Trainee at the Antenna and Submillimetre Wave Group at European Space Research and Technology Centre, ESTEC in the Netherlands. In 2005, Vanja joined Sony Ericsson Mobile Communications (now Sony Mobile Communications) and is currently a Senior Research Engineer in the Communications and Networking Group. Her research interests comprise smart antenna systems and their implementation in compact mobile devices. Vanja Plicanic has participated in the European research initiative COST 2100.

Henrik Asplund received the M.S. degree from Uppsala University, Sweden in 1996. In the same year he joined Ericsson Research, Stockholm, Sweden, where he is currently involved in research on the antenna and propagation aspects of wireless communication systems. His research interests include measurement and modeling of mobile radio channels, multi-antenna systems and MIMO, and interference alignment. Henrik Asplund has participated in the European research initiatives COST 259, COST 273, and COST 2100 and is currently participating in the FP7 HIATUS research project.

Buon Kiong Lau (S'00–M'03–SM'07) received the B.E. degree (with honors) from the University of Western Australia, Perth, Australia and the Ph.D. degree from Curtin University of Technology, Perth, in 1998 and 2003, respectively, both in electrical engineering.

During 2000 to 2001, he worked as a Research Engineer with Ericsson Research, Kista, Sweden. From 2003 to 2004, he was a Guest Research Fellow at the Department of Signal Processing, Blekinge Institute of Technology, Sweden. Since 2004, he has been at the Department of Electrical and Information Technology, Lund University, where he is now an Associate Professor. He has been a Visiting Researcher at the Department of Applied Mathematics, Hong Kong Polytechnic University, China, Laboratory for Information and Decision Systems, Massachusetts Institute of Technology, and Takada Laboratory, Tokyo Institute of Technology, Japan. His primary research interests are in various aspects of multiple antenna systems, particularly the interplay between antennas, propagation channels and signal processing.

Dr. Lau is an Associate Editor for the IEEE TRANSACTIONS ON ANTENNAS AND PROPAGATION and a Guest Editor of the 2012 Special Issue on MIMO Technology for the same journal. From 2007 to 2010, he was a Co-Chair of Subworking Group 2.2 on "Compact Antenna Systems for Terminals" (CAST) within EU COST Action 2100. Since 2011, he has been a Swedish national delegate and the Chair of Subworking Group 1.1 on "Antenna System Aspects" within COST IC1004. He is also the Regional Delegate of European Association on Antennas and Propagation (EurAAP) for Iceland, Norway, Sweden.